Applied Science, Computing and Energy, 2026, 4(3), 441-460

Sol-Gel Synthesis and Characterization of Carbonated Hydroxyapatite Nanoparticles from Chicken Bone Waste for the Remediation of Malachite Green Dye Contamination of Water

James Okon Effiong, Anduang Ofuo Odiongenyi, Uwem Udosen Ubong, Aniefiok Effiong Ite, and Henrietta Ijeoma Kelle

Received: 23 January 2026/Accepted: 03 May 2026/Published: 10 May 2026

Abstract: *The increasing generation of poultry waste and the growing demand for sustainable biomaterials have stimulated interest in the valorization of animal bone residues as precursors for hydroxyapatite (HA) synthesis. In this study, calcium hydroxyapatite nanoparticles were synthesized from chicken bone waste using a sol–gel method followed by calcination, and the resulting material was comprehensively characterized using pH monitoring, Energy Dispersive X-ray Spectroscopy (EDX), Fourier Transform Infrared Spectroscopy (FTIR), Scanning Electron Microscopy (SEM), UV–Visible spectroscopy, Brunauer–Emmett–Teller (BET) analysis, and Density Functional Theory (DFT) pore size distribution. The synthesis process showed effective gel formation, with pH increasing from approximately 4.0 to 11.1 during NaOH addition, indicating favorable conditions for hydroxyapatite precipitation. EDX analysis revealed that calcium, phosphorus, and oxygen were the dominant elements, with atomic concentrations of 45.02%, 12.05%, and 36.74%, respectively. The material exhibited a Ca/P ratio of 3.74 and an estimated hydroxyapatite content of approximately 63%, suggesting the coexistence of hydroxyapatite with minor calcium-rich phases. FTIR spectra displayed characteristic phosphate bands at 959.79, 1013.83, and 1086.52 cm^{-1}, carbonate bands at 1410.79 and 1457.39 cm^{-1}, and a hydroxyl stretching band at 3570.79 cm^{-1}, confirming the formation of carbonated hydroxyapatite. SEM micrographs revealed agglomerated nanoparticles with rough and porous surfaces. UV–Visible analysis showed enhanced absorbance across the 200–600 nm wavelength range, indicating increased surface activity and defect-related electronic transitions. DFT pore size distribution demonstrated predominant pore diameters between 1.8 and 2.8 nm, with maximum pore volume occurring within the 2.5–2.7 nm range, confirming a mesoporous structure. The BET adsorption model exhibited excellent linearity ($R^2 \approx 0.998$), indicating significant surface accessibility and adsorption potential. The combined characterization results confirmed the successful conversion of chicken bone waste into mesoporous carbonated hydroxyapatite nanoparticles possessing high surface reactivity, functionalized phosphate and hydroxyl groups, and desirable physicochemical properties. The synthesized material shows strong potential for applications in environmental remediation, adsorption technologies, catalysis, drug delivery, and bone tissue engineering while providing a sustainable route for poultry waste valorization.*

Keywords: *Hydroxyapatite nanoparticles; Chicken bone waste; Sol–gel synthesis; Mesoporous materials; Waste valorization*

James Okon Effiong
Department of Chemistry, Akwa Ibom State University, Ikot Akpaden, Mkpat Enin LGA, Akwa Ibom State, Nigeria.
Email: effiongjames2020@gmail.com

Anduang Ofuo Odiongenyi
Department of Chemistry, Akwa Ibom State University, Ikot Akpaden, Mkpat Enin LGA, Akwa Ibom State, Nigeria.
Email: anduangodiongenyi@aksu.edu.ng
https://orcid.org/0000-0002-6842-9976

Uwem Udosen Ubong
Department of Chemistry, Akwa Ibom State University, Ikot Akpaden, Mkpat Enin LGA, Akwa Ibom State, Nigeria.
Email: uwemubong@aksu.edu.ng
https://orcid.org/0000-0003-4227-6091

Aniefiok Effiong Ite
Department of Chemistry, Akwa Ibom State University, Ikot Akpaden, Mkpat Enin LGA, Akwa Ibom State, Nigeria.
Email: aniefiokite@aksu.edu.ng
https://orcid.org/0000-0002-5065-7540

Henrietta Ijeoma Kelle
Department of Chemistry, National Open University of Nigeria, Abuja, Nigeria.
Email: hkelle@noun.edu.ng
https://orcid.org/0000-0003-3701-4652

1.0 Introduction

The increasing discharge of industrial effluents into aquatic environments has become one of the most pressing environmental challenges worldwide. Among the various pollutants released into water bodies, synthetic dyes constitute a significant class of contaminants due to their extensive use in textile, paper, printing, leather, pharmaceutical, cosmetic, and food-processing industries. Malachite green (MG), a triphenylmethane cationic dye, is widely employed because of its excellent colouring properties, low cost, and antimicrobial activity. However, the persistence, toxicity, mutagenicity, teratogenicity, and carcinogenicity of malachite green have raised serious concerns regarding its release into aquatic ecosystems. Even at low concentrations, malachite green can reduce light penetration, inhibit photosynthesis, disrupt aquatic food chains, and pose severe health risks to humans and animals through bioaccumulation. Consequently, the development of efficient, sustainable, and economically viable technologies for the removal of malachite green from contaminated water remains an important research priority.

Among the available wastewater treatment technologies, adsorption has emerged as one of the most effective methods because of its simplicity, high removal efficiency, ease of operation, low energy requirements, and adaptability to different wastewater compositions. The performance of adsorption systems is largely dependent on the physicochemical properties of the adsorbent, including its surface area, pore structure, crystallinity, particle size, and surface functional groups. Therefore, considerable efforts have been devoted to developing low-cost, environmentally friendly adsorbents from renewable and waste-derived resources.

Hydroxyapatite (HA), chemically represented as $Ca_{10}(PO_4)_6(OH)_2$, has attracted significant attention as an advanced functional material due to its unique physicochemical properties. Hydroxyapatite constitutes approximately 60–70% of the inorganic component of natural bone and teeth and exhibits excellent biocompatibility, bioactivity, biodegradability, ion-exchange capability, and adsorption properties (Pokhrel, 2018; Munir et al., 2022). These attributes have enabled its application in bone tissue engineering, orthopedic implants, drug delivery systems, catalysis, photocatalysis, environmental remediation, and water treatment technologies. The presence of hydroxyl and phosphate groups within the hydroxyapatite lattice provides numerous active sites for the adsorption of organic and inorganic pollutants, while its porous structure facilitates mass transfer and enhances adsorption performance.

Recent advances in nanotechnology have further increased interest in hydroxyapatite nanoparticles because nanoscale materials exhibit higher surface area, improved porosity, enhanced reactivity, and superior adsorption capabilities compared with their bulk counterparts. Peng et al. (2015) synthesized

carbonated hydroxyapatite nanoparticles with dimensions ranging from 1.9–14.2 nm in diameter and 4.0–36.9 nm in length and reported structures comparable to natural bone apatite. Similarly, Abdelmoaty and Mousa (2024) produced hydroxyapatite nanorods with particle sizes between 11 and 15 nm and a specific surface area of 146 m^2 g^{-1}, demonstrating the importance of mesoporosity and nanostructuring in enhancing the functional performance of hydroxyapatite materials. The increasing emphasis on nanostructured hydroxyapatite has therefore stimulated the search for sustainable precursor materials capable of producing highly porous and reactive hydroxyapatite nanoparticles.

Conventionally, hydroxyapatite is synthesized from high-purity chemical reagents, which often involve expensive processing routes and generate secondary environmental burdens. To overcome these limitations, researchers have increasingly explored waste-derived calcium and phosphorus sources for hydroxyapatite production. Such approaches align with circular economy principles by transforming waste streams into high-value functional materials while reducing environmental pollution. Numerous waste materials, including phosphogypsum, poultry manure, animal bones, eggshells, snail shells, marine shells, and industrial residues, have been successfully converted into hydroxyapatite (Alaneme et al., 2025; Jursene et al., 2025; Maritza et al., 2026; Oladele et al., 2024).

Among these waste resources, animal bones represent one of the most promising precursors because they naturally contain calcium phosphate minerals with compositions closely resembling hydroxyapatite. Chicken bone waste is particularly attractive due to the rapid growth of the global poultry industry and the corresponding increase in bone waste generation. Large quantities of chicken bones are discarded annually in slaughterhouses, restaurants, poultry processing facilities, and households, contributing to environmental pollution and landfill accumulation (Vinoth Kumar et al., 2021). The recovery of calcium and phosphorus from these wastes for hydroxyapatite production offers a sustainable pathway for waste valorization and resource conservation.

Several studies have demonstrated the feasibility of synthesizing hydroxyapatite from poultry-derived wastes. Setiawan et al. (2026) synthesized hydroxyapatite from chicken bones through thermal processing and obtained an optimum yield of 69% with a Ca/P ratio of 1.69. Adji et al. (2025) reported that chicken bones contain approximately 18.9% calcium and 13.9% phosphorus and can be effectively transformed into hydroxyapatite suitable for veterinary applications. Alaneme et al. (2025) synthesized hydroxyapatite from poultry manure and observed Ca/P ratios ranging from 1.28 to 1.71, while FTIR and XRD analyses confirmed the formation of hydroxyapatite as the dominant phase. Similarly, Tosun et al. (2021) successfully recovered phosphorus from animal wastes and produced carbonated hydroxyapatite nanoparticles, demonstrating the feasibility of resource recovery from agricultural waste streams.

The source of the biological precursor significantly influences the structural and functional properties of the resulting hydroxyapatite. Mkhitaryan et al. (2026) reported that hydroxyapatite derived from bovine, porcine, and ostrich bones exhibited different crystallite sizes, porosities, and mechanical properties. Likewise, Balabadra et al. (2024) observed notable differences in the structural and antibacterial properties of hydroxyapatite synthesized from marine shells and fish bones, while Oladele et al. (2024) demonstrated that hydroxyapatite obtained from snail shells exhibited superior reinforcement properties compared with eggshell-derived hydroxyapatite. These findings indicate that precursor origin plays a

crucial role in determining the morphology, porosity, crystallinity, and adsorption characteristics of hydroxyapatite materials.

The synthesis method also significantly influences the final properties of hydroxyapatite. Various techniques, including calcination, precipitation, hydrothermal processing, alkaline hydrolysis, microwave-assisted synthesis, and sol–gel methods, have been employed for hydroxyapatite fabrication (Okpe et al., 2024). Among these approaches, the sol–gel method offers several advantages, including molecular-level homogeneity, precise compositional control, low processing temperatures, enhanced purity, uniform particle size distribution, and the formation of highly porous nanostructures. Furthermore, the sol–gel process promotes the formation of carbonated hydroxyapatite, which closely resembles biological apatite and possesses improved bioactivity and adsorption characteristics (Peng et al., 2015; Tosun et al., 2021).

The environmental applications of hydroxyapatite have expanded considerably in recent years. Bone-derived hydroxyapatite has demonstrated remarkable efficiency in removing toxic heavy metals from water. Rashed et al. (2025) reported removal efficiencies exceeding 99% for Pb^{2+} and Cd^{2+} ions using chemically activated hydroxyapatite synthesized from chicken and camel bones. In addition, hydroxyapatite-based materials have shown excellent catalytic and photocatalytic properties. Petcu et al. (2026) demonstrated that porous hydroxyapatite-containing catalysts synthesized from bone waste can effectively support catalytic reactions, while Alanazi et al. (2026) achieved 99.15% degradation of methylene blue dye using Ag-decorated hydroxyapatite composites under solar irradiation. These studies suggest that nanostructured hydroxyapatite possesses substantial potential for wastewater treatment applications.

Despite these advances, most previous studies have concentrated on biomedical applications, heavy metal adsorption, catalyst development, or basic physicochemical characterization of hydroxyapatite materials. Limited studies have investigated the synthesis of mesoporous carbonated hydroxyapatite nanoparticles from chicken bone waste using the sol–gel method specifically for the remediation of malachite green dye-contaminated water. Furthermore, comprehensive relationships among elemental composition, surface chemistry, morphology, pore structure, and adsorption potential remain insufficiently understood. Few studies have integrated advanced characterization techniques such as Energy Dispersive X-ray Spectroscopy (EDX), Fourier Transform Infrared Spectroscopy (FTIR), Scanning Electron Microscopy (SEM), UV–Visible spectroscopy, Brunauer–Emmett–Teller (BET) surface area analysis, and Density Functional Theory (DFT) pore size distribution to evaluate hydroxyapatite synthesized from poultry waste for dye adsorption applications.

Therefore, the aim of this study was to synthesize mesoporous carbonated hydroxyapatite nanoparticles from chicken bone waste using a sol–gel approach and to comprehensively characterize the synthesized material using EDX, FTIR, SEM, UV–Visible spectroscopy, BET analysis, and DFT pore size distribution. The synthesized nanoparticles were subsequently evaluated for their potential application in the remediation of malachite green dye-contaminated water.

The significance of this study is threefold. First, it provides an environmentally sustainable strategy for the valorization of chicken bone waste, thereby reducing the environmental burden associated with poultry waste disposal. Second, it contributes to the development of low-cost and efficient adsorbent materials for wastewater treatment, particularly for the removal of hazardous dye contaminants. Third, it advances the

understanding of the relationships between synthesis conditions, nanostructure, porosity, surface chemistry, and adsorption performance in waste-derived hydroxyapatite materials. The findings are expected to contribute to the broader goals of sustainable resource recovery, circular economy implementation, environmental remediation, and the development of advanced functional nanomaterials.

2.0 Materials and Methods

2.1 Materials

Waste chicken bones were collected from local poultry processing outlets. Hydrochloric acid (HCl, analytical grade), sodium hydroxide (NaOH, analytical grade), ethanol (99.5%), and deionized water were used throughout the study. All reagents were of analytical grade and were used without further purification.

2.2 Collection and Preparation of Chicken Bone Precursor

Chicken bones were thoroughly washed with tap water to remove adhering flesh, fats, blood, and other impurities. The cleaned bones were subsequently rinsed several times with deionized water and dried in a hot-air oven at 105 °C for 24 h. The dried bones were crushed using a laboratory grinder and sieved to obtain a fine powder.

The powdered bone sample was subjected to thermal treatment in a muffle furnace at 800 °C for 4 h to eliminate residual organic matter and convert the mineral content into a calcium-rich inorganic precursor. After calcination, the sample was allowed to cool to room temperature in a desiccator and subsequently ground into a fine powder for sol–gel synthesis.

2.3 Synthesis of Hydroxyapatite Nanoparticles by Sol–Gel Method

The synthesis of hydroxyapatite nanoparticles was carried out using a modified sol–gel process. Approximately 10 g of calcined chicken bone powder was dispersed in 100 mL of 1.0 M hydrochloric acid under continuous magnetic stirring. The acid treatment facilitated dissolution of calcium-containing species from the calcined bone matrix, resulting in the formation of a homogeneous calcium-rich solution.

The pH of the suspension was continuously monitored during acidification. The addition of hydrochloric acid reduced the pH from approximately 5.0 to 2.1, indicating effective dissolution of calcium compounds.

Following complete dissolution, the solution was filtered to remove insoluble residues. The filtrate was then subjected to controlled neutralization using 1.0 M sodium hydroxide solution added dropwise under vigorous stirring. The pH gradually increased and stabilized at approximately 11.0, indicating favorable conditions for hydroxyapatite nucleation and precipitation.

The resulting suspension was continuously stirred for 4 h to ensure complete hydrolysis and condensation reactions. The formed sol was aged at room temperature for 24 h to facilitate gel formation and structural stabilization. The gel was subsequently dried at 100 °C for 12 h to remove physically adsorbed water and residual solvents.

The dried gel was calcined in a muffle furnace at 800 °C for 3 h to improve crystallinity and produce hydroxyapatite nanoparticles. After cooling, the calcined material was pulverized and stored in airtight containers for characterization.

2.4 Monitoring of Sol–Gel Formation

The progression of the sol–gel process was monitored through pH measurements during both acidification and alkalization stages. A calibrated digital pH meter was used to record changes in pH as hydrochloric acid and sodium hydroxide were added. The pH evolution was used to assess dissolution, hydrolysis, nucleation, and precipitation phenomena occurring during hydroxyapatite formation.

2.5 Characterization of Synthesized Hydroxyapatite Nanoparticles

2.5.1 Energy Dispersive X-ray Spectroscopy (EDX)

The elemental composition of the synthesized nanoparticles was determined using Energy Dispersive X-ray Spectroscopy (EDX) coupled to a scanning electron microscope. The analysis was conducted to quantify the relative concentrations of calcium, phosphorus, oxygen, and trace elements present in the sample. The Ca/P ratio was calculated from the elemental composition to evaluate the degree of hydroxyapatite formation and compare it with stoichiometric hydroxyapatite.

2.5.2 Fourier Transform Infrared Spectroscopy (FTIR)

The functional groups present in the synthesized material were identified using Fourier Transform Infrared Spectroscopy (FTIR). Spectra were recorded within the wavenumber range of 400–4000 cm^{-1} at room temperature. Characteristic absorption bands corresponding to phosphate (PO_4^{3-}), carbonate (CO_3^{2-}), and hydroxyl (OH^-) groups were used to confirm hydroxyapatite formation and evaluate possible ionic substitutions within the crystal lattice.

2.5.3 Scanning Electron Microscopy (SEM)

The surface morphology and particle characteristics of the synthesized hydroxyapatite nanoparticles were investigated using Scanning Electron Microscopy (SEM). Prior to imaging, samples were mounted on conductive carbon tape and coated with a thin conductive layer to minimize charging effects. Micrographs were obtained at various magnifications to examine particle size distribution, agglomeration behavior, surface texture, and porosity.

2.5.4 UV–Visible Spectroscopy

Optical properties of the synthesized nanoparticles were evaluated using a UV–Visible spectrophotometer. Approximately 0.01 g of sample was dispersed in ethanol and sonicated to obtain a homogeneous suspension. The absorbance spectra were recorded over the wavelength range of 200–600 nm using ethanol as the blank reference. The absorption behavior was used to assess surface activity and electronic transitions associated with the hydroxyapatite nanoparticles.

2.5.5 Nitrogen Adsorption–Desorption Analysis

The textural properties of the synthesized nanoparticles were investigated through nitrogen
adsorption–desorption measurements. Prior to analysis, samples were degassed under vacuum at elevated temperature to remove adsorbed moisture and gases.

The specific surface area was determined using the Brunauer–Emmett–Teller (BET) method while the BET surface area was calculated using the equation that relates the Avogadro;s number , , surface area of the adsorbate, molar volume and monolayer adsorption volume (Eddy *et al*., 2025a-c)

2.5.6 Density Functional Theory (DFT) Analysis

Pore size distribution and pore volume characteristics were evaluated using Density Functional Theory (DFT) analysis of the nitrogen adsorption isotherm data. The DFT model was employed because it accurately describes gas adsorption behavior in nanoporous materials by accounting for molecular interactions between adsorbate molecules and pore walls.

The differential pore volume distribution was also calculated as the ratio of pore volume to pore diameter. The DFT analysis was used to determine the dominant pore diameter range, pore volume distribution, and mesoporous characteristics of the synthesized hydroxyapatite nanoparticles (Eddy *et al*., 2026; Nuhu *et al*., 2025)

2.6 Data Analysis

All experimental measurements were performed in triplicate, and results were expressed as mean values. Spectroscopic, morphological, compositional, optical, and adsorption data obtained from FTIR, SEM, EDX, UV–Visible, BET, and DFT analyses were correlated to evaluate the physicochemical properties of the synthesized hydroxyapatite nanoparticles and assess their suitability for environmental and biomedical applications.

3.0 Results and Discussion

3.1 Sol–Gel Formation and pH Evolution During Synthesis

The pH profile obtained during the sol–gel synthesis of calcium hydroxyapatite nanoparticles is presented in Fig. 1. The addition of HCl resulted in a rapid decrease in pH from approximately 5.0 to about 2.1, indicating effective acidification of the precursor suspension and dissolution of calcium-containing species from the calcined chicken bone matrix. Acid treatment promotes the conversion of insoluble calcium compounds into soluble ionic species, thereby facilitating homogeneous mixing and subsequent gel formation.

In contrast, gradual addition of NaOH caused a progressive increase in pH from approximately 4.0 to values exceeding 11.0. The sharp increase observed between pH 7 and 10 indicates the onset of nucleation and precipitation reactions involving calcium and phosphate ions. The stabilization of pH at approximately 11 suggests completion of hydrolysis and condensation reactions leading to gel formation. Alkaline conditions are known to favor hydroxyapatite crystallization by enhancing phosphate ion availability and promoting the formation of Ca–O–P linkages. The observed pH behavior therefore confirms successful sol–gel processing and provides evidence for the formation of a calcium phosphate network that subsequently transformed into hydroxyapatite during calcination.

3.2 Elemental Composition and Chemical Purity of the Synthesized Nanoparticles

3.2.1 EDX Analysis

The elemental composition of the synthesized nanoparticles determined by EDX analysis is presented in Table 1. Calcium and oxygen were the dominant elements, accounting for 45.02 and 36.74 at.% respectively, while phosphorus constituted 12.05 at.%. The predominance of calcium, phosphorus, and oxygen confirms the formation of a calcium phosphate material consistent with hydroxyapatite.

Table 1 shows that trace amounts of Mg, Al, Si, Fe, K, S, Sn, and Ba were also detected. These elements originate primarily from the natural composition of chicken bone and minor contamination introduced during processing. The presence of magnesium and silicon is particularly noteworthy because both elements are known to substitute within the hydroxyapatite lattice and can enhance biological performance, bioactivity, and osteoconductivity.

The calculated atomic Ca/P ratio based on the EDX data is approximately 3.74, which is considerably higher than the stoichiometric hydroxyapatite value of 1.67 (Baizhan *et al*., 2023). This elevated ratio suggests the presence of additional calcium-rich phases such as calcium oxide (CaO) and calcium carbonate ($CaCO_3$), likely formed during calcination. Similar observations have been reported for biogenic hydroxyapatite obtained from animal bones, where thermal treatment partially decomposes carbonate-containing mineral phases, resulting in calcium enrichment (Eknapakul, *et al*., 2024).

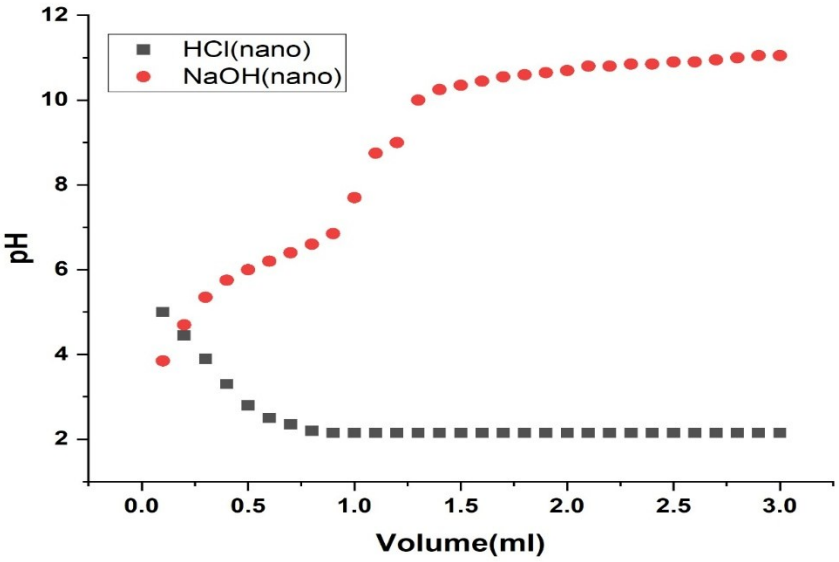

Fig. 1: Plot for Variation of pH with volume of HCl and NaOH for the determination of pH at zero charge for calcium hydroxyapatite produce from chicken bone using sol gel method

3.2.2 Comparison with Expected Hydroxyapatite Composition

The compositional comparison presented in Table 2 indicates that the sol–gel-derived chicken bone sample contains approximately 59.1% calcium and 15.8% phosphorus, corresponding to an estimated hydroxyapatite content of about 63%.

Table 1 : EDX data for nanoparticles (Nano) obtained from sol gel method after calcination of chicken bone

Element Number	Element Symbol	Element Name	Atomic Conc.	Weight Conc.
15	P	Phosphorous	12.05	11.09
13	Al	Aluminum	1.17	1.03
12	Mg	Magnesium	1.06	0.03
14	Si	Silicon	0.52	0.42
50	Sn	Tin	0.19	0.20
56	Ba	Barium	0.10	0.23
16	S	Sulfur	0.25	0.30
20	Ca	Calcium	45.02	45.00
19	K	Potassium	0.27	0.20
8	O	Oxygen	36.74	33.29
26	Fe	Iron	0.74	0.60

Table 2: Comparison of Percentage Composition of Calcium Hydroxyapatite Nanoparticles and Impurities in Fish Bone, Crude Chicken Bone, and Sol–Gel Chicken Bone Samples

Sample Type	Ca (%)	P (%)	Ca/P Ratio	Estimated HA Composition (%)	Major Impurities (%)	Likely Phases Present
Chicken Bone (Sol–Gel + Calcination)	59.1	15.8	3.74	~63% Hydroxyapatite	Mg (0.8), Si (0.9), Fe (0.5), Al (0.3), trace Ba	HA + CaO + $CaCO_3$ + doped HA

The relatively high hydroxyapatite fraction demonstrates that the sol–gel method effectively converted chicken bone waste into a valuable calcium phosphate nanomaterial (Tan *et al*., 2026). However, the elevated Ca/P ratio and the presence of minor impurities suggest that the product is not entirely phase-pure hydroxyapatite. Instead, the material likely consists of hydroxyapatite coexisting with calcium oxide, calcium carbonate, and ion-substituted hydroxyapatite phases.

Such compositional features are advantageous in several biomedical and environmental applications. Carbonated and ion-substituted hydroxyapatites often exhibit higher dissolution rates, greater surface reactivity, and enhanced adsorption capacity compared with stoichiometric hydroxyapatite (Argatu *et al*., 2026). Consequently, the synthesized nanoparticles may possess improved performance in bone tissue engineering, pollutant adsorption, and catalyst-support applications.

3.3 Functional Group Characterization by FTIR Spectroscopy

The FTIR spectrum of the synthesized nanoparticles is shown in Fig. 2, while the major absorption bands are summarized in Table 3.

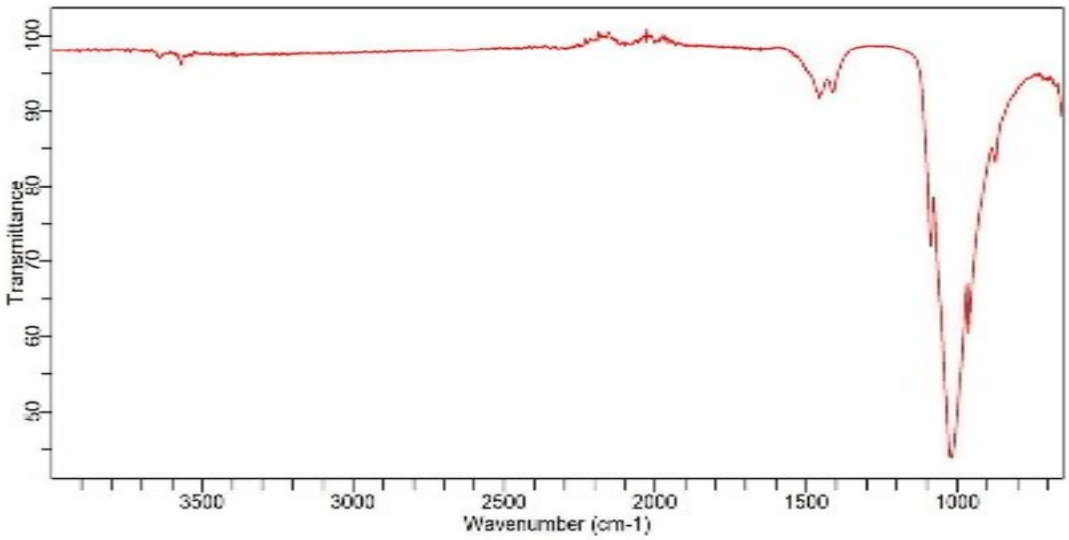

Fig. 2 FTIR spectrum of calcium hydroxyapatite nanoparticles synthesised from chicken bone by sol gel method

A strong absorption band at 959.79 cm^{-1} corresponds to the ν_1 symmetric stretching vibration of phosphate (PO_4^{3-}) groups. This peak is a characteristic signature of hydroxyapatite and confirms the presence of the phosphate framework within the crystal lattice. Additional phosphate-related bands observed at 1013.83 and 1086.52 cm^{-1} are attributed to ν_3 asymmetric stretching vibrations of phosphate ions. The strong intensity of the 1086.52 cm^{-1} band further confirms extensive phosphate incorporation and successful hydroxyapatite formation.

Table 3|:FTIR Peak Positions, Intensities, Bond Types, Assignments, and References of Calcium Hydroxyapatite Nanoparticles Obtained from Chicken Bone by Sol-Gel Method (Nano)

Peak No.	Wavenumber (cm^{-1})	Intensity	Bond Type	Mode of Vibration	Functional Group / Assignment	Structural Relevance	Reference
1	959.79	0.24198	P–O	ν_1 symmetric stretch	PO_4^{3-} group	Confirms phosphate skeleton of HA lattice	Elliott, 1994
2	1013.83	0.00000	P–O	ν_3 asymmetric stretch	PO_4^{3-} group (very weak)	Suggests reduced intensity due to nanocrystallinity	Fleet, 2009
3	1086.52	0.48175	P–O	ν_3 asymmetric stretch	PO_4^{3-} group	Strong phosphate incorporation in nano-HA	Vallet-Regí et al., 2001
4	1410.79	0.92621	C–O	ν_3 asymmetric stretch	CO_3^{2-} group (B-type substitution)	Carbonate incorporation enhances bioactivity	Patiño et al., 2009
5	1457.39	0.92048	C–O	ν_3 asymmetric stretch	CO_3^{2-} group (B-type substitution, broadened)	Indicates carbonate substitution typical of bioapatite	Suryanarayana et al., 2008
6	3570.79	0.92926	O–H	Stretching vibration	OH^- group (hydroxyl in HA lattice)	Structural hydroxyls enhance stability & adsorption	Elliott, 1994

Two prominent bands located at 1410.79 and 1457.39 cm^{-1} correspond to carbonate (CO_3^{2-}) vibrations. These peaks indicate B-type carbonate substitution, in which carbonate ions replace phosphate ions within the hydroxyapatite structure. Carbonate substitution is a characteristic feature of naturally derived apatites and closely resembles the mineral composition of biological bone. The occurrence of carbonate groups supports the EDX findings and suggests the presence of carbonated hydroxyapatite.

A broad absorption band at 3570.79 cm^{-1} is assigned to hydroxyl (OH^-) stretching vibrations. The presence of structural hydroxyl groups confirms the formation of hydroxyapatite rather than other calcium phosphate phases such as tricalcium phosphate. Hydroxyl groups contribute significantly to

lattice stability, ion exchange behavior, and adsorption properties.

Overall, the FTIR results provide strong evidence for successful synthesis of carbonated hydroxyapatite nanoparticles and confirm the coexistence of phosphate, carbonate, and hydroxyl functional groups that are characteristic of naturally derived hydroxyapatite.

3.4 Morphological Characteristics of the Nanoparticles

The SEM micrographs presented in Figs, 3 and 4 reveal the surface morphology of the synthesized hydroxyapatite nanoparticles. The images show irregularly shaped agglomerates composed of fine particulate structures distributed across the surface.

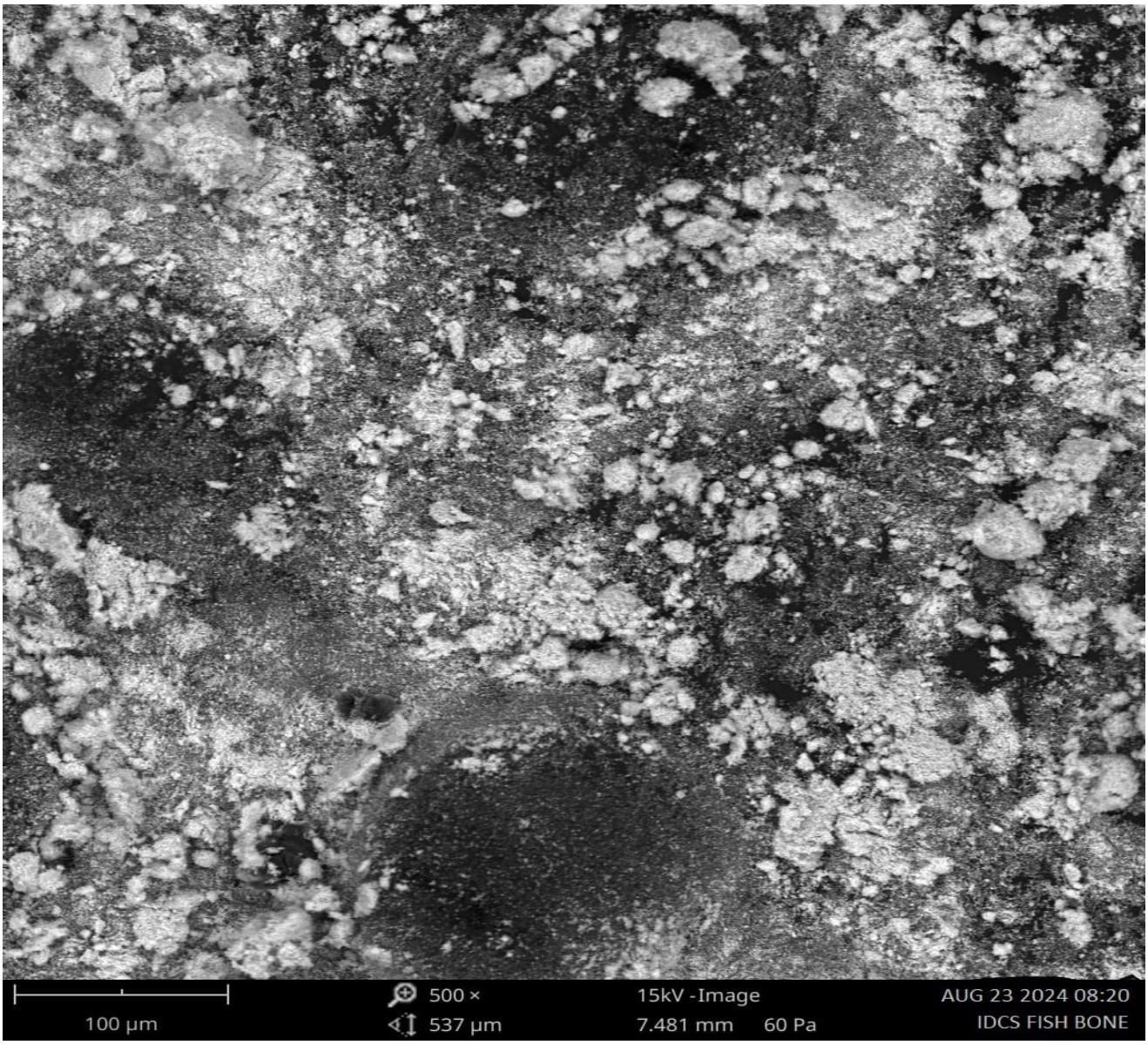

Fig. 3: Scanning electron micrograph of nanoparticles (at 500 x magnification) synthesized from fish bone by sol gel method

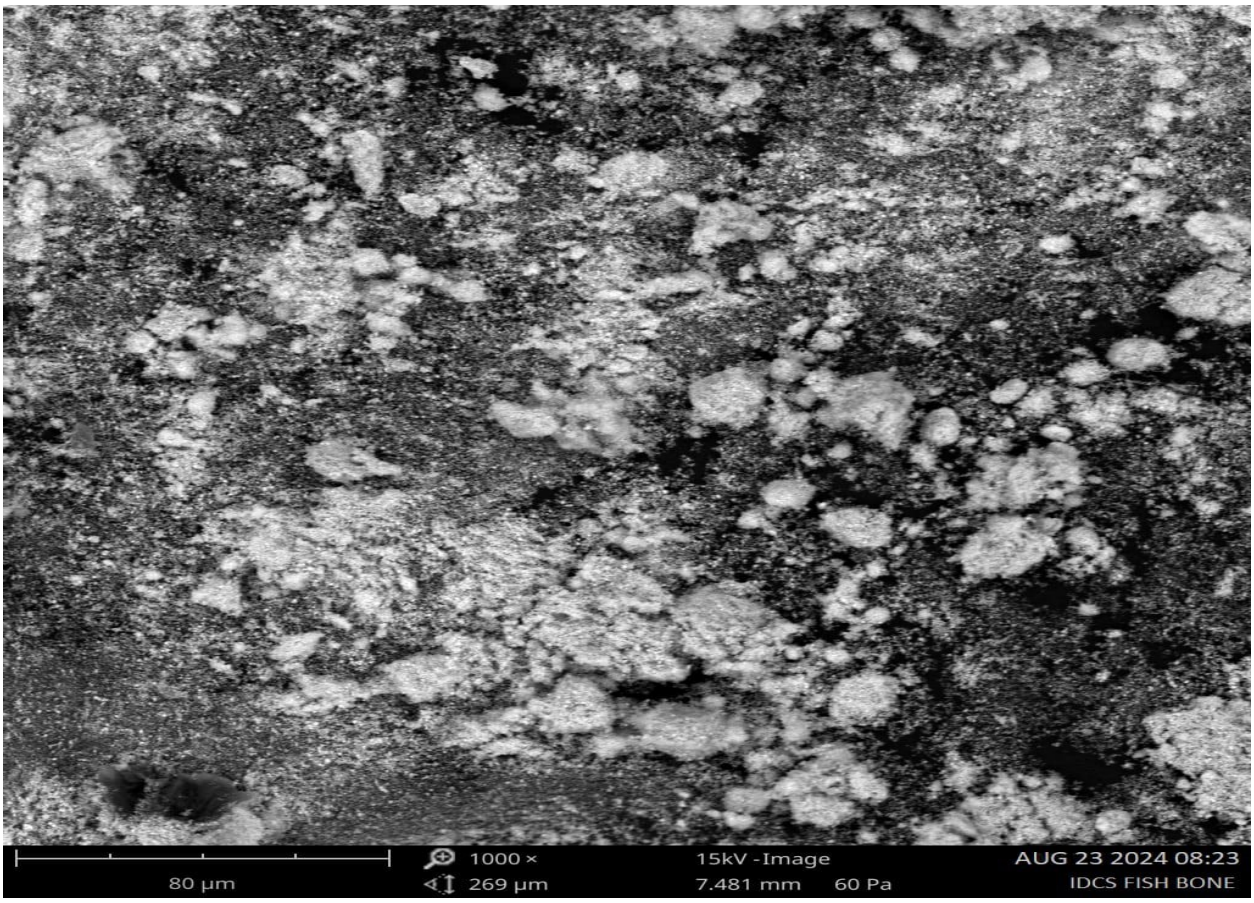

Fig. 4 : Scanning electron micrograph of nanoparticles (at 1000 x magnification) synthesized from fish bone by sol gel method

The particles appear clustered into dense aggregates, a phenomenon commonly observed in nanocrystalline hydroxyapatite due to high surface energy and strong interparticle interactions. The agglomerated morphology suggests that particle growth occurred through nucleation followed by coalescence during drying and calcination. Despite aggregation, numerous fine crystalline domains can be observed throughout the micrographs, indicating successful nanoscale material formation.

The rough and porous surface texture evident in the SEM images is advantageous for adsorption and biomedical applications. Increased surface roughness provides a larger active surface area, enhances ion exchange capacity, and promotes cellular attachment when used as a biomaterial. Furthermore, the heterogeneous surface structure is consistent with the presence of carbonate-substituted hydroxyapatite and minor secondary calcium phases identified by EDX and FTIR analyses. The morphology therefore confirms that the sol–gel process produced a highly porous nanostructured material with substantial surface activity.

3.5 Optical Properties of the Sol–Gel Hydroxyapatite Nanoparticles

The UV–Visible absorption spectrum shown in Fig, 5 compares the absorbance characteristics of the sol–gel product with the ethanol blank. The synthesized material exhibits consistently higher absorbance throughout the investigated

wavelength range (200–600 nm), indicating significant interaction between electromagnetic radiation and the nanoparticle surface.

Strong absorption in the ultraviolet region is attributed to electronic transitions associated with phosphate groups and defect sites within the hydroxyapatite lattice. The gradual decrease in absorbance with increasing wavelength reflects reduced photon energy and lower transition probability in the visible region.

The broad absorption profile suggests the existence of surface defects, carbonate substitutions, and trace metal dopants identified by EDX analysis. These structural features create localized energy states that enhance light absorption. The higher absorbance of the sol–gel sample relative to the ethanol blank confirms successful nanoparticle formation and indicates the potential suitability of the material for photocatalytic, sensing, and environmental remediation applications.

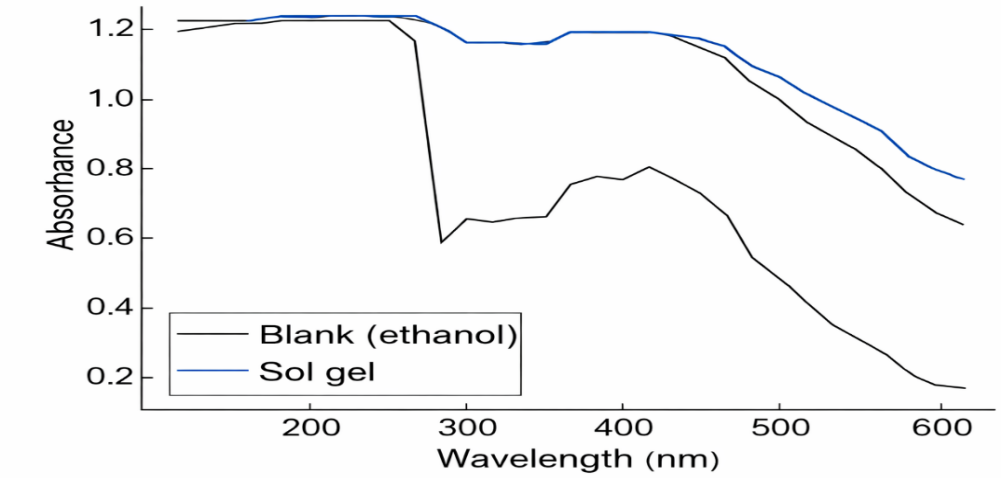

Fig. 5: UV visible absorption spectrum of calcium hydroxyapatite using ethanol as the blank

3.6 Correlation of Characterization Results

The characterization results collectively confirm the successful synthesis of calcium hydroxyapatite nanoparticles from chicken bone waste using the sol–gel method. The pH evolution study demonstrated appropriate conditions for gel formation and hydroxyapatite precipitation. EDX analysis verified the predominance of calcium, phosphorus, and oxygen, while FTIR spectroscopy confirmed the presence of phosphate, carbonate, and hydroxyl groups characteristic of hydroxyapatite. SEM observations revealed agglomerated nanostructures with rough and porous surfaces, and UV–Visible spectroscopy demonstrated enhanced optical absorption behavior.

The combined evidence indicates that the synthesized material consists predominantly of carbonated hydroxyapatite containing minor calcium-rich and trace element-substituted phases. Such structural characteristics closely resemble natural bone mineral and enhance the potential utility of the material in biomedical, environmental remediation, adsorption, and catalytic applications.

3.7 Surface Area and Pore Structure Analysis by Density Functional Theory (DFT)

The pore size distribution and adsorption characteristics of the hydroxyapatite nanoparticles synthesized from chicken bone by the sol–gel method were further investigated using Density Functional Theory (DFT) and

Brunauer–Emmett–Teller (BET) analyses. The DFT pore size distribution curve and BET plot are presented in Figures 6 and 7, respectively.

3.7.1 DFT Pore Size Distribution

The DFT pore size distribution (Fig. 6) reveals that the synthesized hydroxyapatite possesses pores predominantly within the range of approximately 1.8–2.8 nm. The highest pore volume contribution was observed at pore diameters between 2.5 and 2.7 nm, where the differential pore volume (dV(d)) reached values of approximately 0.12–0.14 $cm^3\ g^{-1}\ nm^{-1}$. The DFT pore size distribution function can be expressed as dV/dD with (V) = cumulative pore volume,(D) = pore diameter, and dV/dD) = differential pore volume distribution.
ant.

The DFT approach calculates pore dimensions by fitting adsorption data to statistical mechanical models that describe gas adsorption within pores of varying geometries. Unlike the Barrett–Joyner–Halenda (BJH) method, DFT accounts for molecular interactions between adsorbate molecules and pore walls, making it particularly suitable for nanoporous materials.
According to IUPAC classification, pores with diameters less than 2 nm are micropores, whereas pores between 2 and 50 nm are mesopores. The observed pore distribution therefore indicates that the synthesized material contains a mixture of microporous and mesoporous domains, with mesopores being domin

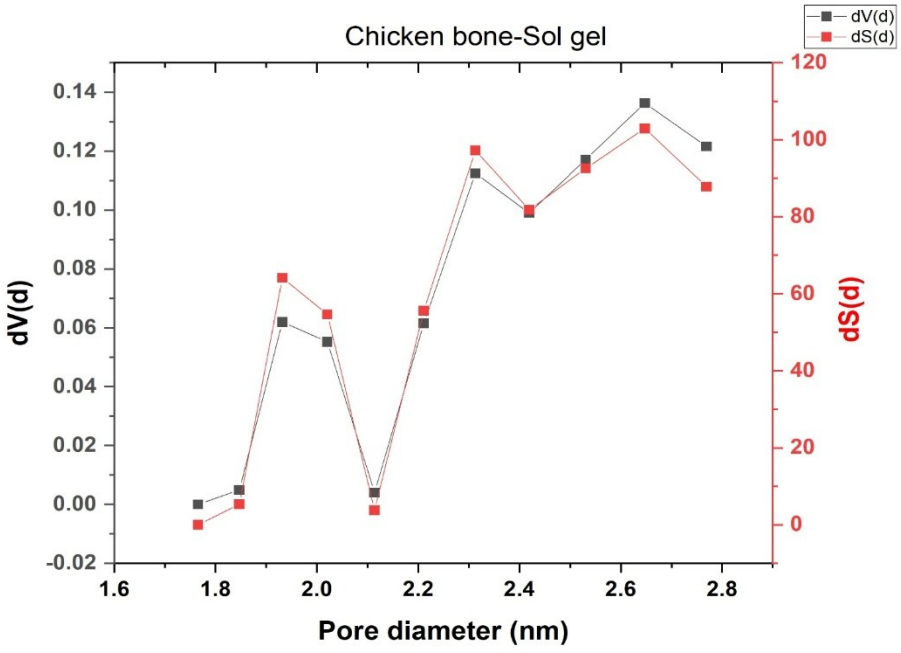

Fig. 6: DFT plot for the calcium hydroxyapatite nanoparticles produced from chicken bone by sol gel method

The concentration of pores around 2.3–2.7 nm demonstrates that the sol–gel synthesis route produced a highly porous nanostructure. Such pore dimensions are advantageous because they provide increased surface accessibility, enhanced adsorption sites, and improved mass transport characteristics. Similar mesoporous hydroxyapatite structures have been reported to

exhibit superior adsorption capacities for heavy metals, dyes, and pharmaceutical contaminants due to their large internal surface area and interconnected pore network.

The presence of nanoscale pores also supports the SEM observations, which revealed rough and porous agglomerated structures. Thus, both SEM and DFT analyses consistently indicate the development of a highly porous hydroxyapatite framework following calcination.

3.7.2 BET Surface Area Determination

The BET plot obtained from nitrogen adsorption measurements is shown in Fig. 7. The BET equation is expressed as equation 1

$$\frac{1}{V(P/P_p-1)} = \frac{1}{V_m C} + \frac{C-1}{V_m C}\left(\frac{P}{P_0}\right) \qquad (1)$$

where V = volume of adsorbed nitrogen, V_m = monolayer adsorption capacity, P = equilibrium pressure, P_0 = saturation pressure, and C = BET constant

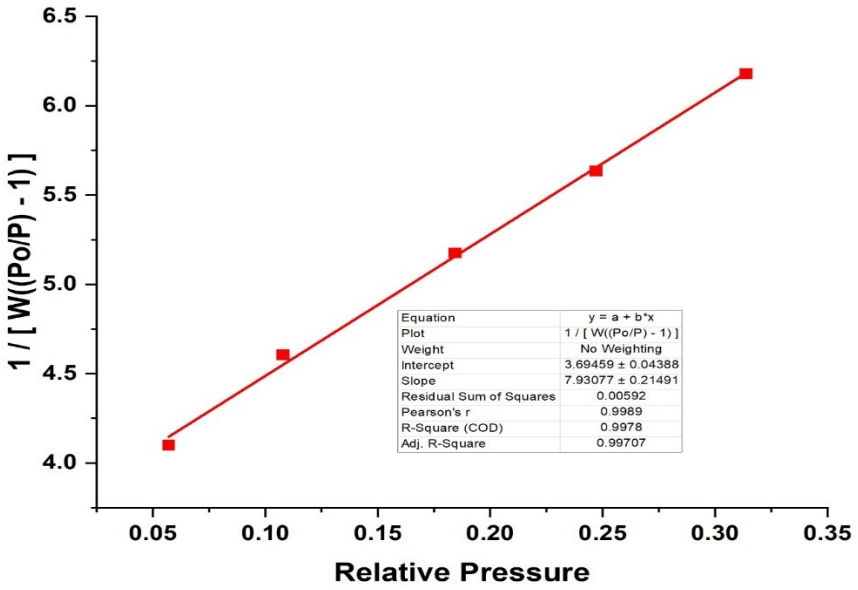

Fig. 7: BET adsorption isotherm for the calcium hydroxyapatite produced from chicken bone

The linearized BET plot exhibits excellent linearity within the relative pressure range investigated, yielding a coefficient of determination ((R^2)) of approximately 0.998. The high correlation coefficient indicates that monolayer adsorption assumptions are valid and that the experimental data are well described by the BET model.

The BET surface area wasis calculated using equation 2

$$S_{BET} = \frac{V_m N_A \sigma}{22414} \qquad (2)$$

where (S_{BET}) = specific surface area ($m^2\ g^{-1}$), N_A = Avogadro's number, σ = cross-sectional area of nitrogen molecule (0.162 nm^2), and V_m = monolayer adsorption volume.

The positive slope and strong linear behavior indicate efficient nitrogen adsorption over the hydroxyapatite surface, suggesting the existence of abundant accessible adsorption sites. Such characteristics are typical of nanocrystalline hydroxyapatite possessing high porosity and substantial external surface area.

3.7.3 Correlation Between DFT Results and Other Characterization Parameters

The DFT results are in excellent agreement with the findings obtained from SEM, FTIR, EDX, and UV–Visible analyses.

First, the nanoscale pore dimensions observed by DFT are consistent with the rough and highly porous morphology observed in SEM micrographs. SEM revealed agglomerated particles separated by void spaces and channels, while DFT quantitatively confirmed that these voids correspond predominantly to mesopores within the 2–3 nm range.

Second, the significant porosity revealed by DFT provides a structural explanation for the strong adsorption behavior inferred from FTIR analysis. The presence of hydroxyl (OH^-), phosphate (PO_4^{3-}), and carbonate (CO_3^{2-}) functional groups creates chemically active adsorption sites. The high density of mesopores increases the accessibility of these functional groups, thereby enhancing adsorption performance.

Third, the elevated calcium content and carbonated hydroxyapatite structure identified by EDX and FTIR are known to promote pore formation during calcination. Decomposition of residual organic matter and carbonate-containing species generates gaseous products that create additional pore channels within the material. This mechanism explains the mesoporous structure observed by DFT.

Fourth, the UV–Visible spectrum showed enhanced absorbance across the UV and visible regions. Such optical behavior is often associated with increased surface defects, higher surface area, and greater density of active sites. The high porosity and surface accessibility demonstrated by DFT therefore provide a plausible explanation for the enhanced optical response of the synthesized nanoparticles.

3.7.4 Implications of the DFT Characteristics for Applications

The Density Functional Theory (DFT) pore size distribution analysis, together with the BET surface characterization, revealed that the synthesized hydroxyapatite nanoparticles possess a highly porous mesostructured architecture with numerous accessible adsorption sites. The pore size distribution was dominated by pores within the 2–3 nm range, indicating the presence of well-developed mesopores. Such pore dimensions are advantageous because they facilitate the rapid diffusion of ions, dye molecules, and other contaminants into the internal structure of the material while simultaneously maintaining a high specific surface area available for adsorption processes.

The mesoporous nature of the synthesized hydroxyapatite is expected to enhance its performance in environmental remediation applications. The large number of accessible surface active sites and interconnected pore channels provide favorable conditions for the adsorption of heavy metals, dyes, and other organic pollutants from aqueous solutions. The high surface area also makes the material a suitable support for catalytic systems, as improved pore accessibility promotes efficient mass transfer and increases the availability of catalytic active sites.

Furthermore, the pore characteristics observed from the DFT analysis suggest potential utility in biomedical applications. The mesopores can serve as reservoirs for the loading and controlled release of therapeutic agents, making the material a promising candidate for drug delivery systems. In addition, the porous hydroxyapatite framework can facilitate nutrient transport, protein adsorption, cell adhesion, and tissue ingrowth, which are desirable characteristics for bone tissue engineering and regenerative medicine.

Overall, the DFT and BET results demonstrate that the sol–gel synthesis route successfully converted chicken bone waste into

nanostructured hydroxyapatite with a well-developed mesoporous architecture and high adsorption potential. These findings are consistent with the structural, compositional, and morphological characteristics established through FTIR, EDX, SEM, and UV–Visible spectroscopic analyses. The strong agreement among the various characterization techniques provides compelling evidence for the successful synthesis of functional carbonated hydroxyapatite nanoparticles with physicochemical properties suitable for advanced environmental remediation, adsorption, catalytic, and biomedical applications.

4.0 Conclusion

This study successfully demonstrated the conversion of chicken bone waste into calcium hydroxyapatite (HA) nanoparticles through a sol–gel synthesis route followed by calcination. The pH evolution during synthesis confirmed effective dissolution, hydrolysis, condensation, and precipitation processes required for hydroxyapatite formation. Characterization results collectively established the successful production of a calcium phosphate nanomaterial with properties comparable to naturally derived bioapatite.

EDX analysis revealed that calcium, phosphorus, and oxygen were the dominant elements in the synthesized material, confirming the formation of a calcium-rich phosphate phase. The calculated Ca/P ratio of 3.74 suggested the coexistence of hydroxyapatite with minor calcium-rich phases such as CaO and $CaCO_3$. Trace amounts of Mg, Si, Fe, and Al were detected, indicating the formation of ion-substituted hydroxyapatite structures that may enhance the material's functional properties.

FTIR spectroscopy confirmed the characteristic phosphate, hydroxyl, and carbonate functional groups associated with hydroxyapatite. The presence of B-type carbonate substitution demonstrated that the synthesized product closely resembles biological apatite, thereby improving its potential bioactivity and adsorption performance. SEM observations revealed agglomerated nanoparticles with rough and porous surfaces, indicative of high surface reactivity and abundant active sites.

Nitrogen adsorption studies further demonstrated that the material possesses a predominantly mesoporous structure with pore diameters concentrated between 2.0 and 3.0 nm. The DFT pore size distribution and BET analysis confirmed the existence of a highly porous network with significant adsorption capacity and excellent surface accessibility. These findings were consistent with the porous morphology observed by SEM and the enhanced optical absorption behaviour observed in the UV–Visible spectra.

The strong agreement among EDX, FTIR, SEM, UV–Visible, DFT, and BET analyses confirms that the sol–gel process is an effective and sustainable approach for producing nanostructured hydroxyapatite from chicken bone waste. The synthesized material exhibits desirable chemical composition, functional groups, porosity, and surface characteristics suitable for biomedical applications, environmental remediation, adsorption processes, catalyst support systems, and advanced functional materials. The study therefore provides a valuable pathway for waste valorization while generating a high-value hydroxyapatite nanomaterial with significant industrial and environmental relevance.

5.0 References

Abdelmoaty, A., & Mousa, S. (2024). Synthesis and characterization of hydroxyapatite nanoparticles from calcium hydroxide fouled with gases evolved from smokestack of glass industry. *Scientific Reports, 14*, 10969.

https://doi.org/10.1038/s41598-024-60970-2

Adji, D., Sutrisno, B., Prastiwi, A., Anggoro, D., & Wuryastuti, H. (2025). Sustainable synthesis of hydroxyapatite from poultry waste for veterinary applications: A calcination approach. *Open Veterinary Journal, 15*(4), 1695–1701. https://doi.org/10.5455/OVJ.2025.v15.i4.21

Alanazi, A. H., Atta, A., Bilel, H., Halawani, R. F., Aloufi, F. A., Al Zbedy, A. S., & Nassar, A. M. (2026). Biogenic fabrication of Ag-NPs@hydroxyapatite from goat bone waste: A sustainable route for photocatalytic and antioxidant applications. *Inorganics, 14*(1), 2. https://doi.org/10.3390/inorganics14010002

Alaneme, K. K., Oke, S. R., Fagbayi, S. B., Alabi, O. O., Ojo, O. M., Kareem, S. A., & Folorunso, D. O. (2025). Synthesis and structural analysis of calcined poultry manure for hydroxyapatite development. *Next Sustainability, 5*, 100079. https://doi.org/10.1016/j.nxsust.2024.100079

Alsharif, S. A., Badran, M. I., Moustafa, M. H., Meshref, R. A., & Mohamed, E. I. (2023). Hydrothermal extraction and physicochemical characterization of biogenic hydroxyapatite nanoparticles from buffalo waste bones for in vivo xenograft in experimental rats. *Scientific Reports, 13*(1), 17490. https://doi.org/10.1038/s41598-023-43989-9

Argatu, D., Georgescu, A., Luchian, I., Curca, F. R., Scutariu, M. M., Budala, D. G., Tofan, N., Constantin, V., Cojocaru, C., & Bida, F. C. (2026). Hydroxyapatite-based biomaterials in dentistry: Functional performance and clinical relevance—A narrative review. *Oral, 6*(3), 58. https://doi.org/10.3390/oral6030058

Baizhan, D., Sagdoldina, Z., Buitkenov, D., Kambarov, Y., Nabioldina, A., Zhumabekova, V., & Bektasova, G. (2023). Study of the structural-phase state of hydroxyapatite coatings obtained by detonation spraying at different O_2/C_2H_2 ratios. *Crystals, 13*(11), 1564. https://doi.org/10.3390/cryst13111564

Balabadra, K. M., Selvam, S. P., Ramadoss, R., & Sundar, S. (2024). Hydroxyapatite synthesis and characterization from marine sources: A comparative study. *Journal of Oral Biology and Craniofacial Research, 14*(6), 706–711. https://doi.org/10.1016/j.jobcr.2024.09.009

Eddy, N. O., Garg, R., Ukpe, R. A., Ameh, P. O., Gar, R., Musa, R., Kwanchi, D., Wabaidur, S. M., Afta, S., Ogbodo, R., Aikoye, A. O., & Siddiqu, M. (2024c). Application of periwinkle shell for the synthesis of calcium oxide nanoparticles and in the remediation of Pb^{2+}-contaminated water. *Biomass Conversion and Biorefinery*. https://doi.org/10.1007/s13399-024-05285-y

Eddy, N. O., Garg, R., Garg, R., Ngwu, C., Ekele, D. O., Awe, F. E., Ukpe, R. A., & Ogbonna, I. (2024d). Experimental and theoretical investigations of crab shell-based CaO nanoparticles for the photodegradation of penicillin G in water. *International Journal of Environmental Science and Technology*. https://doi.org/10.1007/s13762-024-06214-2

Eddy, N. O., Jibrin, J. I., Ukpe, R. A., Odiongenyi, A., Iqbal, A., Kasiemobi, A. M., Oladele, J. O., & Runde, M. (2024b). Experimental and theoretical investigations of photolytic and photocatalysed degradations of crystal violet dye (CVD) in water by oyster shell-derived CaO nanoparticles (CaO-NP). *Journal of Hazardous Materials Advances, 13*, 100413. https://doi.org/10.1016/j.hazadv.2024.100413

Eddy, N. O., Oladede, J., Eze, I. S., Garg, R., Garg, R., & Paktin, H. (2024a). Synthesis and characterization of CaO nanoparticles from periwinkle shell for the treatment of tetracycline-contaminated water by adsorption and photocatalyzed degradation. *Results in Engineering*, 103374. https://doi.org/10.1016/j.rineng.2024.103374

Eddy, N. O., Udeokpote, G. C., Ekele, D. O., Garg, R., Garg, R., & Paktin, H. (2026). Synthesis of carbon quantum dots using unutilized low-grade lignite coal. *BMC Chemistry*. https://doi.org/10.1186/s13065-026-01798-x

Eknapakul, T., Jiamprasertboon, A., Amonpattaratkit, P., Pimsawat, A., Daengsakul, S., Tanapongpisit, N., Saenrang, W., Bootchanont, A., Wannapraphai, P., Phetrattanarangsi, T., Boonchuduang, T., Khamkongkaeo, A., & Yimnirun, R. (2024). Unraveling the structural complexity of and the effect of calcination temperature on calcium phosphates derived from *Oreochromis niloticus* bones. *Heliyon, 10*(8), e29665. https://doi.org/10.1016/j.heliyon.2024.e29665

Ibekwe, C. A., Oyatogun, G. M., Esan, T. A., & Oziegbe, E. O. (2026). Synthesis and characterization of hydroxyapatite from dolomite-based source for bone regeneration. *American Journal of Biomedical Engineering, 14*(1), 9–15. https://doi.org/10.5923/j.ajbe.20261401.02

Jursene, E., Michailova, L., Jureviciute, S., Stankeviciute, Z., Grigoraviciute, I., & Kareiva, A. (2025). Synthesis and characterization of calcium hydroxyapatite from waste phosphogypsum. *Materials, 18*(12), 2869. https://doi.org/10.3390/ma18122869

Maritza, N., Dewanti, B. S. D., & Yuliatun, L. (2026). Precipitation, synthesis, and characterization of hydroxyapatite derived from gonggong snail shells (*Strombus canurium*). *Indonesian Journal of Chemistry, 26*(2). https://doi.org/10.22146/ijc.107110

Mkhitaryan, L., Baghdasaryan, L., Nazaretyan, K., Khachatryan, Z., Khachatryan, A., Torosyan, M., Aghayan, M., Rodríguez, M. A., & Rstakyan, V. (2026). Valorization of bone waste: Effect of animal bone origin on hydroxyapatite structure and properties. *Environmental Science and Pollution Research, 33*(7), 2921–2935. https://doi.org/10.1007/s11356-026-37460-1

Munir, M. U., Salman, S., Ihsan, A., & Elsaman, T. (2022). Synthesis, characterization, functionalization and bio-applications of hydroxyapatite nanomaterials: An overview. *International Journal of Nanomedicine, 17*, 1903–1925. https://doi.org/10.2147/IJN.S360670

Nuhu, J. S., Awe, F. E., Garg, R., Garg, R., Eddy, N. O., & Paktin, H. (2025). Cobalt titanate nanocatalyst for enhanced photodegradation of atrazine: Kinetics, degradation efficiency, and mechanistic analysis. *BMC Chemistry, 19*(31). https://doi.org/10.1186/s13065-025-01394-5

Okpe, P. C., Folorunso, O., Aigbodion, V. S., & Obayi, C. (2024). Hydroxyapatite synthesis and characterization from waste animal bones and natural sources for biomedical applications. *Journal of Biomedical Materials Research Part B: Applied Biomaterials, 112*(7), e35440. https://doi.org/10.1002/jbm.b.35440

Oladele, I. O., Taiwo, A. S., & Olubambi, P. A. (2024). Characterization of animal shells-derived hydroxyapatite reinforced epoxy bio-composites. *High Performance Polymers, 36*(3), 285–297. https://doi.org/10.1177/26349833231223984

Peng, H., Wang, J., Lv, S., Wen, J., & Chen, J.-F. (2015). Synthesis and characterization of hydroxyapatite nanoparticles prepared by a high-gravity precipitation method. *Ceramics International, 41*(10, Part B), 14340–14349. https://doi.org/10.1016/j.ceramint.2015.07.067

Petcu, G., Patrascu, M., Gheorghe, V.-C., Ionescu, G., Radoiu, M., Magdziarz, A., & Mărculescu, C. (2026). Synthesis of hydroxyapatite-containing catalysts from bone waste—Conventional route versus microwaves. *Catalysis Today, 462*, 115538. https://doi.org/10.1016/j.cattod.2025.115538

Pokhrel, S. (2018). Hydroxyapatite: Preparation, properties and its biomedical applications. *Advances in Chemical Engineering and Science, 8*(4), 225–240. https://doi.org/10.4236/aces.2018.84016

Rashed, M. N., Gad, A. A. M., & Fathy, N. M. (2025). Physiochemical synthesis of hydroxyapatite adsorbents from chicken and camel bone waste for removing Cd and Pb ions from polluted water. *Discovery Water, 5*, 3. https://doi.org/10.1007/s43832-025-00190-5

Setiawan, R. B., Mumtaz, F. Z., Suprianti, L., & Kusuma, R. M. (2026). Synthesis of hydroxyapatite from chicken bones using the high temperature method. *AJARCDE (Asian Journal of Applied Research for Community Development and Empowerment), 10*(1), 1–6. https://doi.org/10.29165/ajarcde.v10i1.869

Tan, S. L., Ng, C. K., Ting, C. H., Yeo, W. H., Ramesh, S., & Tan, C. Y. (2026). A review on biowaste-derived hydroxyapatite composites: Materials, synthesis and 3D printing fabrication methods. *Journal of Materials Research and Technology, 40*, 53–73. https://doi.org/10.1016/j.jmrt.2025.12.104

Tosun, G. U., Sakhno, Y., & Jaisi, D. P. (2021). Synthesis of hydroxyapatite nanoparticles from phosphorus recovered from animal wastes. *ACS Sustainable Chemistry & Engineering, 9*(45), 15117–15126. https://doi.org/10.1021/acssuschemeng.1c01006

Vinoth Kumar, K. C., Jani Subha, T., Ahila, K. G., Ravindran, B., Chang, S. W., Mahmoud, A. H., Mohammed, O. B., & Rathi, M. A. (2021). Spectral characterization of hydroxyapatite extracted from Black Sumatra and Fighting cock bone samples: A comparative analysis. *Saudi Journal of Biological Sciences, 28*(1), 840–846. https://doi.org/10.1016/j.sjbs.2020.11.020

Declaration

Consent for publication

Not Applicable

Availability of data and materials

The publisher has the right to make the data public

Conflict of Interest

The authors declared no conflict of interest

Ethical Considerations

Not applicable

Competing interest

The authors report no conflict or competing interest

Funding

The author declared no source of funding\

Authors' Contributions

James Okon Effiong conceived the study, conducted the experiments, analyzed the data, and prepared the initial manuscript draft. Anduang Ofuo Odiongenyi supervised the research, validated the methodology, and reviewed the manuscript. Uwem Udosen Ubong and Aniefiok Effiong Ite contributed to data interpretation and manuscript revision. Henrietta Ijeoma Kelle assisted with result validation, critical review, and final manuscript editing. All authors approved the final manuscript.